# Approximate analysis of hydrofoil material impact on cavitation inception

ISROMAC 2016
International Symposium on Transport Phenomena and Dynamics of Rotating Machinery
Hawaii, Honolulu
April 10-15, 2016

**Eduard Amromin**[1*]

## Abstract

Flow-induced vibration of hydrofoils affects pressure pulsations on their surfaces and influences cavitation inception and desinence. Because these pulsations depend on the hydrofoil material, cavitation inception and desinence numbers for hydrofoils of the same shape made from the diverse metals are different. This conclusion is based on the comparison of the numerical solutions of the fluid-structure interaction problems with the data of the earlier performed experiments.

## Keywords

Cavitation inception — Fluid-structure interaction - Flow-induced vibration

[1] *Mechmath LLC, Federal Way, WA 98003, USA*
***Corresponding author**: amromin@aol.com

## INTRODUCTION

This paper describes a study of the material impact on the inception and desinence of attached cavitation. The body material impacts on cavitation have been discussed for many decades. In particular, the monograph [1] gives a reference to a paper published in 1944 and considering the body surface cracks as the sources of nucleation and cavitation inception. Recently this idea was used in the numerical analysis [2]. Also, a substantial role of the surface wettability became clear after discovery [3] of the meniscus at the line of cavity detachment on bodies. The comparative experiments [4], [5] with bodies of hydrophilic and hydrophobic surfaces (like illustrated by Fig.1) proved this role.

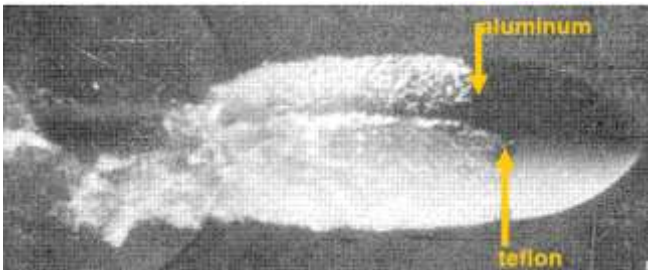


**Figure 1** View of a cavity on ellipsoid composed from two parts with different surface materials (after [4])

This difference in the observed cavity shapes on axisymmetric bodies made from different materials gave a hope to see more significant shape differences for hydrofoils with very smooth pressure distributions in cavitation-free conditions at small angles of attack α. The hydrofoils Cav2003 with various surface materials (Teflon, aluminum, steel) were selected for experiments [6] in Saint Anthony Falls Laboratory. The existence of the detailed experimental study [7] of Cav2003 in another facility also influenced this selection.

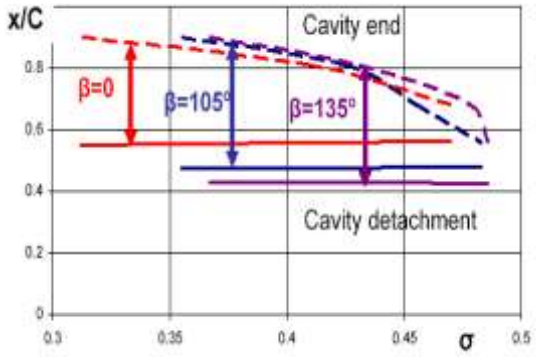


**Figure 2** Computed cavity detachments (solid lines) and ends (dashed lines) on hydrofoils Cav2003 for $C_L$=0.125 at the flow speed 10m/s; β=0 corresponds to hydrophilic surface (metals), other β correspond to hydrophobic surface (as Teflon).

The theory [8] predicted a visible difference in the cavity shapes on Cav2003 (as shown in Fig.2) at small α (lift coefficients $C_L$). This difference is a consequence of wettability impact on cavity detachment. However, in the experiment [6] the attached cavities were covered by drifting bubbles at such α and there was no possibility to validate the prediction. On the other hand, though any substantial impact of the hydrofoil material on cavitation at higher angles of attack was not expected because there is no possibility to affect this detachment at high α, the clear difference of cavitation inception number $\sigma_i$ and cavitation desinence number $\sigma_d$ for two metal hydrofoils

with approximately the same surface wettability (the same contact angle) was suddenly found. As seen in Fig. 3, for the same cavitation number, cavitation inception and desinence occur at significantly smaller angles attack on the aluminum hydrofoil. The difference in these angles starts from 0.5° and can exceed 1°.

It was recalled then that vibration of the hydrofoil tips during water tunnel tests is the well-observed material-dependent phenomenon. Also, an increase of cavitation inception number due to structural vibration was already reported [9]: when the measurements reveal the first torsion eigen-mode, the cavitation inception number significantly increased. So, a study of the structural vibration impact on cavitation of the hydrofoil Cav2003 inception looks reasonable.

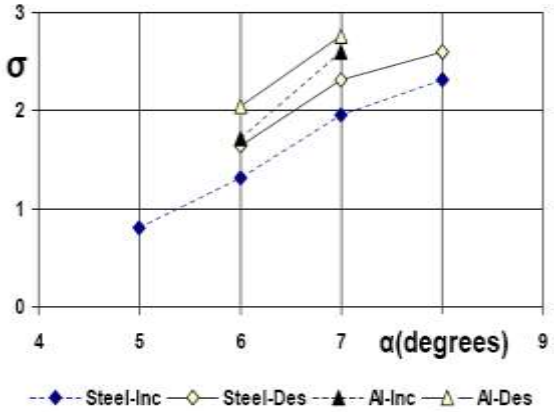


**Figure 3** Observed [6] cavitation inception and desinence numbers for aluminum and steel Cav2003

The presented study provides a four-step analysis of the hypothesis of the vibration impact on cavitation inception and desinence in the experiments [6]. The hydrofoil spanwise deformations in water tunnel turbulent incoming flow are found during the first step. Its chordwise deformations in this flow are found during the second step. The pressure oscillation around the hydrofoils at the resonance frequencies is computed during the third step. Finally, cavitation inception and desinence numbers are computed for actual values of the hydrofoil chord *C* and the incoming flow speed *Uo*.

## 1. THREE-DIMENSIONAL HYDROELASTTIC PROBLEM

One can determine the hydrofoil deformation under a flow impact using the ideal fluid theory. The spanwise vibration can be found employing the strong coupling of equations for beam bending deformation V and torsion deformation *θ*.

$$\frac{E^* I}{U^2}\frac{\partial^4 V}{\partial z^4} - \left(\rho S + m_1\right)(V + X\theta)St^2 - \hat{\rho}\int_0^C F dx = 0 \quad (1)$$

$$\frac{G^*}{U^2}\frac{\partial}{\partial z}\left(J\frac{\partial \theta}{\partial z}\right) + St^2\left[\rho SXV + (I_\theta + m_2)\theta\right] - \hat{\rho}\int_0^C (x - \frac{C}{2})F dx = 0 \quad (2)$$

with Birnbaum equation for the load pulsation $\gamma(x)$ considered in the sections z=const. Here Eqs. (1), (2) are similar to employed in [10] and the Birnbaum equation [11] after regularization [12] is transformed into

$$\gamma^* + \frac{i\omega\Psi(x)}{\pi}\int_0^C\left[\int_0^C \frac{\gamma^* e^{i\omega(\xi-\tau)}}{\pi}\int_{\omega(\tau-\xi)}^{\infty}\frac{e^{i\chi}d\chi}{\chi}d\tau\right]\frac{d\xi}{\Psi(\xi)}$$

$$-\frac{i\omega\Psi(x)}{\pi}\int_0^C\left[(\xi-\frac{C}{2})\theta + V\right]\frac{d\xi}{\Psi(\xi)} = -\frac{\Psi(x)}{\pi}\int_0^C\frac{\partial\Phi_1}{\partial y}\frac{d\xi}{\Psi(\xi)} \quad (3)$$

$E^*$ and $G^*$ are complex elasticity modules; ρ and $\hat{\rho}$ are densities of metal and water; *I*, *J*, $I_\theta$ are the section inertia moments, *S* is its area; $m_1$, $m_2$ are section added masses; *V* and θ are bending and torsion deformations;

$$F = \gamma^* Uo - i\omega\int_0^x \gamma^* d\xi;\ U = \sqrt{1 - Cp};\ \Psi(x) = \sqrt{C/x - 1};$$

*St*=*ωC*/*Uo*; *ω* is the perturbation frequency, $\Phi_1$ is its potential. The equations (1)-(3) are supplemented by the conditions *θ(0)=0; dθ/dz(0)=0; V(0)=0; dV/dz(0)=0; d²V/dz²(λC)=0; d³V/dz³(λC)*=0.

The employed inflow turbulence spectrum (shown in Fig.4) was selected with regards to the usual data for water tunnels [13]. The solution of Eqs.(1)-(3) with this spectrum for a very soft hydrofoil (*Real*{$E^*$}=3Mpa) of the aspect ratio λ=1.27 gave the first bending resonance at 60Hz, whereas the loose coupling computations [10] with Theodorsen spectrum gave it at 59Hz for the same hydrofoil with a very small cavity (let us recall that cavitation can reduce the resonance frequency). The described method gave max|*V*|≈0.0022*C* against max|*V*|≈0.002*C* in [10] at a slightly higher ω.

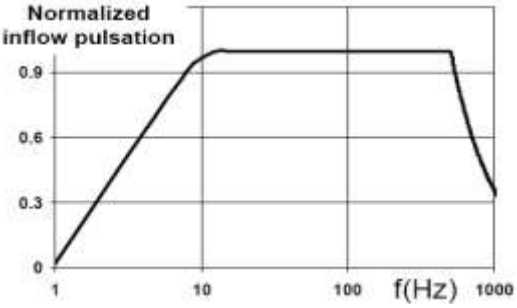


**Figure 4** Excitation spectra for a water tunnel normalized by the maximum harmonic

Some characteristics of the spanwise bending vibration of hydrofoils Cav2003 of *C*=0.08m, and the aspect ratio λ=2.35 at *Uo*=10m/s (as employed in experiments [6]) are shown in Figs.5-7. The aluminum density $\rho$=2800kg/m$^3$, for steel $\rho$=7900kg/m$^3$. The elasticity modulus for aluminum is *Real*{$E^*$}=69Gpa and for the steel *Real*{$E^*$}=180Gpa. The structural loss coefficient 0.02 was selected for metals here.

The material impact on the lift spectra is illustrated by Fig.5. The presented results are normalized by $U_t$=*χ*, where χ is the inflow turbulence intensity. The computations relate to the spatially uniform inflow.

The lift pulsation of the softer aluminum hydrofoil is clearly higher than these pulsations of the steel hydrofoil at the resonances, whereas the situation at other frequencies is invisible in the scale of Fig.5.

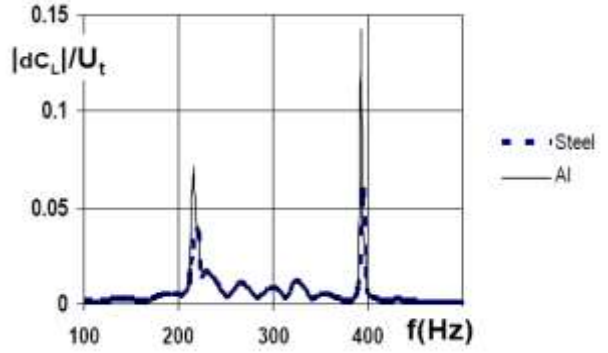


**Figure 5** Computed lift pulsation spectra for aluminum and steel hydrofoils Cav2003 in water tunnel

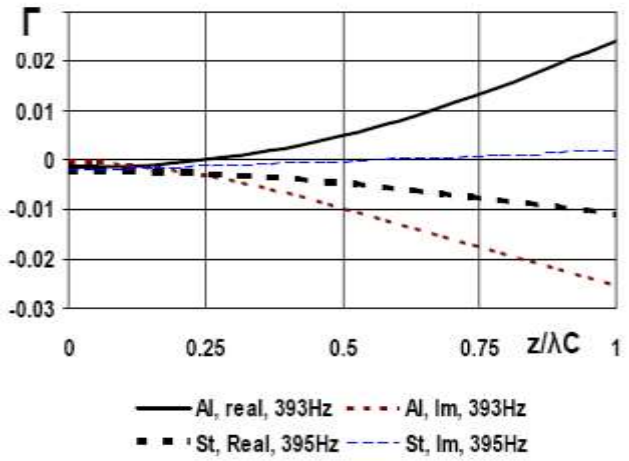


**Figure 6** Effect of material on spanwise load distributions on Cav2003 at resonances in a water tunnel

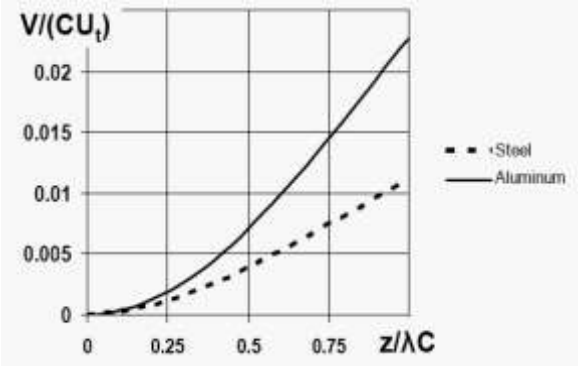


**Figure 7** Hydrofoil spanwise bending deformations at bending resonances

Besides of the total lift oscillations, it is interesting to see the spanwise distributions of the normalized load $\Gamma = \int_0^C \gamma(x,z)dx$. Distributions of the real and imaginary parts of load pulsations on aluminum and steel hydrofoils at their resonances are compared in Fig.6.

The computed bending deformation of the hydrofoils at the resonances in the same water tunnel conditions are shown in Fig.7. It is necessary to note that only bending modes considered in [10] are visible here, whereas the torsion deformations within the considered frequency band ($f$=ω/2π<500Hz) are negligibly small (like in [10]).

The pressure pulsations associated with the spanwise bending are not sufficient to explain differences of σ in Fig.3. So, the chordwise deformation should be analyzed

.

## 2. TWO-DIMENSIONAL HYDROELASTIC PROBLEM

The 2D chordwise bending deformation can be found by solving the equation

$$\frac{E^*}{U^2}\frac{\partial^4}{\partial x^4}\left[\frac{|Y|^3 v}{12}\right] - St^2 \rho Y v + \hat{\rho}\frac{F}{U} = 0 \qquad (1a)$$

together with the regularized Birnbaum equation

$$\gamma^* + \frac{i\omega\Psi(x)}{\pi}\int_0^C\left[\int_0^C \frac{\gamma^* e^{i\omega(\xi-\tau)}}{\pi}\int_{\omega(\tau-\xi)}^{\infty}\frac{e^{i\chi}d\chi}{\chi}d\tau\right]\frac{d\xi}{\Psi(\xi)} - \frac{i\omega\Psi(x)}{\pi}\int_0^C v\frac{d\xi}{\Psi(\xi)} = \frac{\Psi(x)}{\pi}\int_0^C\left(i\omega V - \frac{\partial\Phi_1}{\partial y}\right)\frac{d\xi}{\Psi(\xi)}. \qquad (3a)$$

Here $\gamma^*(x) = \gamma + i\gamma_i$.

The equations (1a), (3a) are supplemented by the conditions $d^2v/dx^2(0)=0$; $d^2v/dx^2(C)=0$; $v(C/2)=V$; $dv/dx(C/2)=\theta$. The value of $V$ in these conditions is found by solving Eqs.(1)-(3) during the previous step of computations.

Let us prove the important advantage of the strong hydroelastic coupling for this study. One may rewrite Eqs.(1a), (3a) in the matrix form as $A_{11}\vec{\gamma}^* + A_{12}\vec{v} = f_1$; $A_{21}\vec{\gamma}^* + A_{22}\vec{v} = f_2$. A resonance occurs when $\|A_{11}\|\|A_{22}\| - \|A_{12}\|\|A_{21}\| = 0$. For the loose coupling $A_{12} = A_{21} = 0$ and therefore such coupling can be inaccurate near resonance frequencies.

One can see in Fig.8 that the deflection of trailing edges of the hydrofoil sections depends on their distance from the hydrofoil tip. Such a dependency of the solutions of Eqs.(1a) and (3a) on $z$ is caused by the dependency of $V$ on $z$ shown in Fig.7. Further, as seen in Fig.9, only a very trailing part of the hydrofoil undergoes the substantial chordwise deformations. These deformations depend on both the hydrofoil material and the real thickness of the trailing edge. This thickness does not go to zero because in the reality the edge is never absolutely sharp.

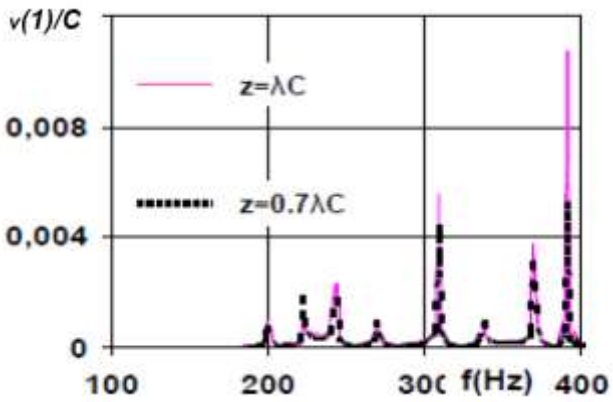


**Figure 8** Deflection of trailing edges of diverse sections of the aluminum Cav2003 in the water tunnel

As illustrated by Fig. 10, the account of the hydrofoil thickness in the vicinity of their trailing edge significantly affects the computed lift pulsation (at least at resonances). Indeed, for the chord $C$=0.08m, the thickness of 0.005$C$ is not realistic and even 0.01$C$ (that is less than 1mm) may be an underestimation of it. Nevertheless, this figure is useful because it shows the certain qualitative effect.

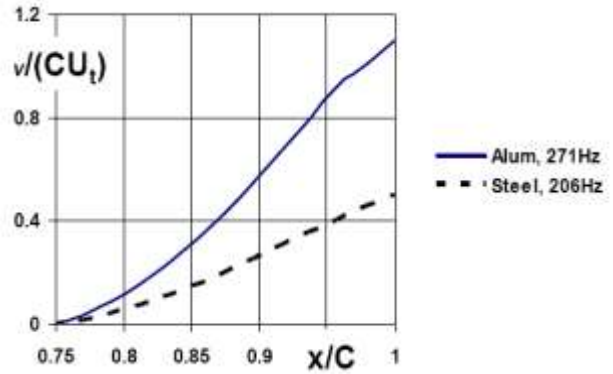


**Figure 9** Chordwise bending deformation of the hydrofoil section at resonances

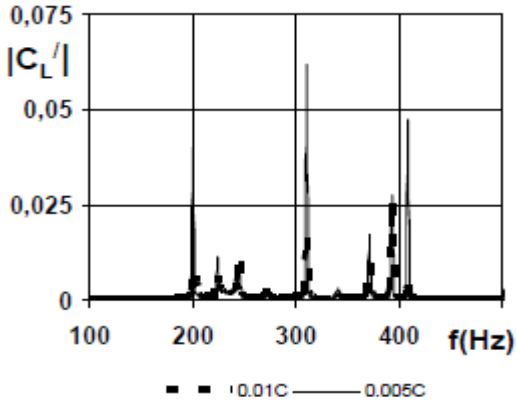


**Figure 10** Example of the impact of trailing edge thickness on lift coefficient pulsation of the tip section of aluminum hydrofoil Cav2003 in the water tunnel

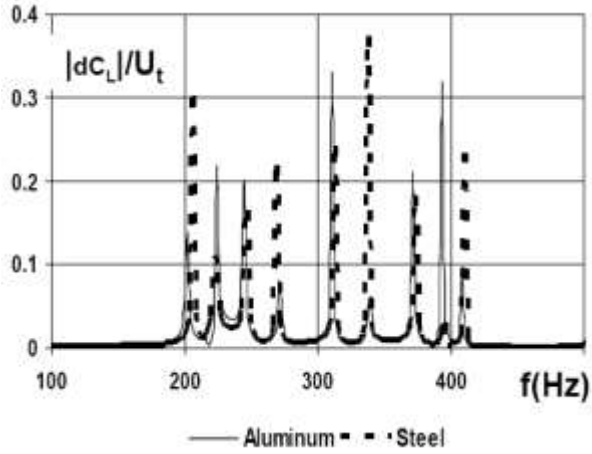


**Figure 11** Impact of material on lift coefficient pulsation of tip section of hydrofoil Cav2003 in a water tunnel

The lift coefficient pulsation near 2D tip section of the 3D foil is substantially greater than its lift coefficient pulsations at the resonance frequencies (shown Fig.5). Also, as seen in Fig.11, lift pulsations are substantially different for sections of aluminum and steel hydrofoils, though their first resonance frequencies are close.

So, as shown above, there are several effects absent for absolutely rigid hydrofoils. These effects have been neglected in the previous studies of cavitation inception.

## 3. COMPUTATION OF PRESSURE OSCILLATIONS

Determination of $\sigma_i$ and $\sigma_d$ first requires compute pressure over the hydrofoil in the unsteady flow. The issue for such computation is in the insufficient information on the real water tunnel inflow. Neither the turbulence magnitude spectrum, nor phases of inflow harmonics are usually known. So, only solutions for perturbations at resonance frequencies would be free of arbitrary assumptions and usable for the further estimations. Also, unlike to the linear dependencies presented in Figs.5, 9 and 11, where results are normalized by $U_t$, the following dependencies should be computed for the certain values of $U_t$ selected from a realistic band.

Further, as proven by measurements [14], [15] in the water tunnel conditions, the hydrofoil resonances with the highest responses usually occur at frequencies lower than 1 kHz. On the other hand, a typical bubble extension time is smaller than $10^{-3}$s. So, cavitation inception and desinence can be analyzed in a quasi-steady approach using the viscous-inviscid interaction method [8], though the pressure along the hydrofoil will be computed with taking into account instant variations of both the section angles of attack and camber lines.

The unsteady pressure distribution will be calculated using Bernoulli equation after determination the velocity potential Φ using the following condition for its normal derivative on the contour S of the hydrofoil sections

$$\left.\frac{\partial\Phi\{x,y,t\}}{\partial N}\right|_S = e^{i\omega t}\left[\frac{\partial\Phi_1\{x\}}{\partial N} - i\omega e^{-i\omega t_{0v}\{x\}}\left|v\{x\}\right|\right]. \quad (4)$$

Here $\omega t_{0v}$ is the phase shift found from solutions of Eqs.(1a),(3a). Additionally to hydrodynamic singularities on S, vortices are distributed behind the hydrofoil, where their intensities are defined in the accordance with Helmholtz theorem.

As in [16], non-permeability of the water tunnel wall is also taken into account in this ideal fluid problem. However, the semi-empirical formula [17]

$$C_L = 2\pi\alpha(1+0.87T)(1-e^{12.5T-0.07}\,\mathrm{Re}^{-0.186})$$

for the lift of symmetric hydrofoils is used here instead of Kutta-Joukovskii condition. Examples of pressure distribution near its leading edge are shown in Fig.12.

The effect of the hydrofoil material on the history of pressure minima of this hydrofoil is illustrated by Fig.13. There the time is normalized by dividing on the ratio *C*/*Uo*. These differences of minima are comparable with the difference of measured cavitation numbers in Fig.3.

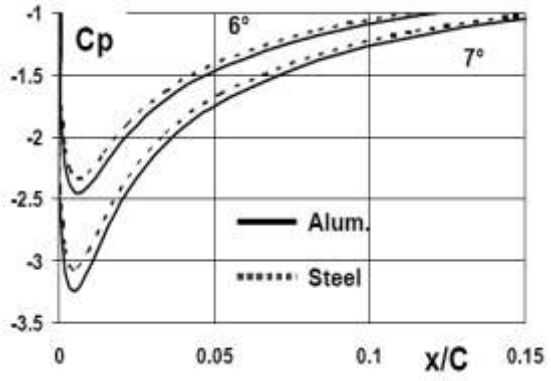


**Figure 12** Pressure distributions near leading edges of hydrofoils made from different materials

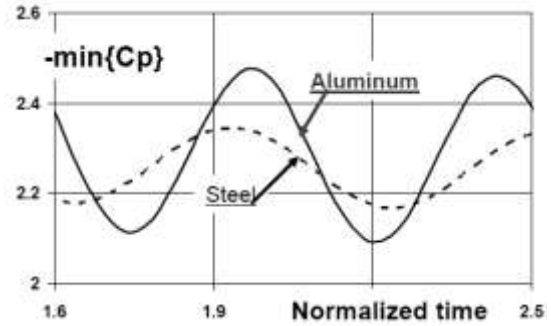


**Figure 13** Histories of *Cp* minima at α=6° for hydrofoils made from different materials.

So, these pressure computations look usable for following estimations.

## 4. ESTIMATION OF CAVITATION INCEPTION AND DESINENCE NUMBERS

Two different models of cavitation are employed here for computation of cavitation inception and cavitation desinence. Determination of $\sigma_d$ is based on the earlier described model of sheet cavitation in viscous fluid with the corresponding viscous-inviscid interaction method [8], [16]. This model (illustrated by the flow sketch in Fig.14) considers sheet cavitation as a specific kind of separated flow. The cavity itself is submerged in the hydrofoil boundary layer and the surface tension influences the equilibrium condition of the meniscus separating the cavity head from water. The maximum of σ for sheet cavity at given *C* and *Re* is considered as $\sigma_d$.

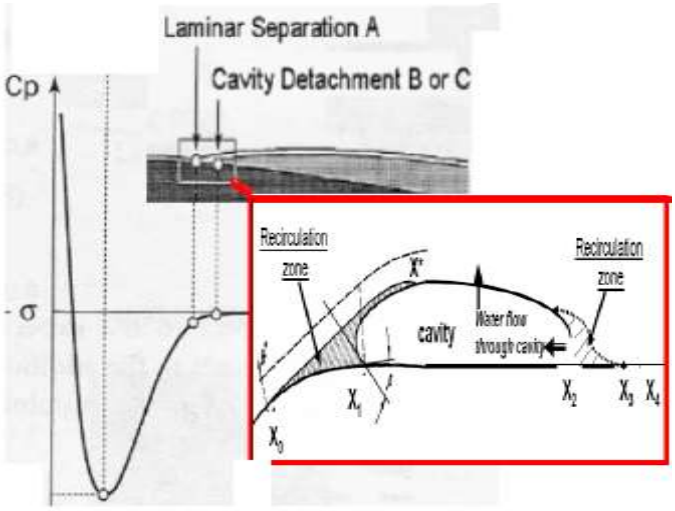


**Figure14** Sketch of an attached cavity

Let us point out that this maximum is smaller than max{-Cp}. This difference of σ and max{-Cp} is in the accordance with experimental data from the review [18] plotted in Fig.15 (in these data initially obtained by 1954 for bodies of various sizes the difference between inception and desinence was not pointed out yet).

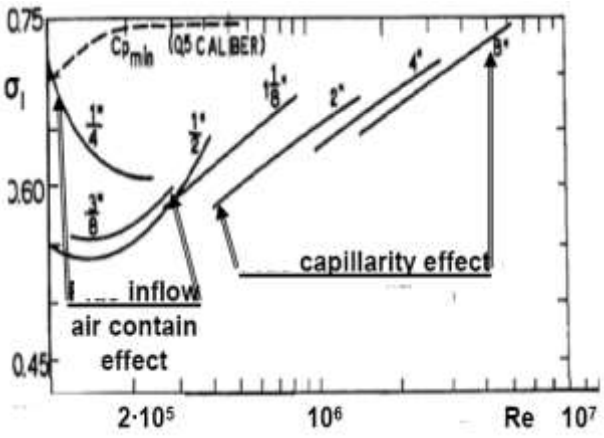


**Figure 15** Experimental dependencies of cavitation inception number on *Re* for axisymmetric bodies with hemi-spherical heads; numbers show body diameters *D*

Vapor cavitation number $\sigma_V = 2(P_\infty - P_V)/\rho U_\infty^2$ was used indeed in this figure instead of the real cavitation number $\sigma = 2(P_\infty - P_C)/\rho U_\infty^2$ because for appearing cavitation it is impossible to measure the sum

$P_C = P_V + P_g$, where $P_g$ is the gas (air) pressure in the cavity. The difference between the real cavitation number employed in computations and vapor cavitation number usually employed in presentations of the experimental data is more substantial at small *Re*, and this circumstance generally affects validation of computational results.

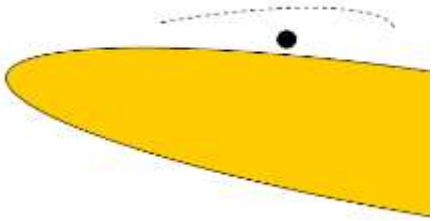

**Figure 16** Sketch of a bubble (the filled circle) in a separation zone near the hydrofoil leading edge (its boundary shown by the dotted line).

In the range of angle of attack presented in Fig.3, cavitation inception on the hydrofoil Cav2003 occurs within viscous separation zones in the vicinity of the trailing edge and in this paper (like in [16]) the computed $\sigma_i$ corresponds to the pressure within a stable spherical bubble drifting in the separation zone at the hydrofoil leading edge, where a recirculating flow region exists (the corresponding sketch is given in Fig.16). The thickness of this zone and the size of bubble (that would not significantly disturb the flow there) depends on *Re*, whereas the difference of pressure in the bubble and outside it depends on surface tension. The employed method of computation of flow in such zones was already described [19], but a supplementary comparison of the computed and measured [20], [21] velocities in zones of viscous separation is given in Fig.17.

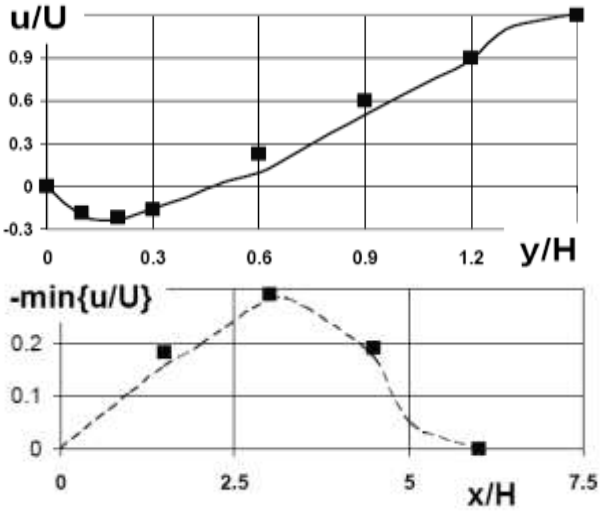


**Figure 17** Computed (lines) and measured velocities across (in the top, with data [19]) and along (in the bottom, with data [20]) separation zones.

Because it was difficult to find similar data for separation zones on hydrofoils, the data for another separating flow were used here. Further, the computed cavitation inception and desinence numbers are compared in Fig.18 for conditions of the experiment [7]. The measured $\sigma_d$ was plotted there with indication of the experimental discrepancy of data. Two symbols for the same α show the cavitation desinence numbers for the top side and the bottom side of this symmetric hydrofoil; their difference is unexplained yet.

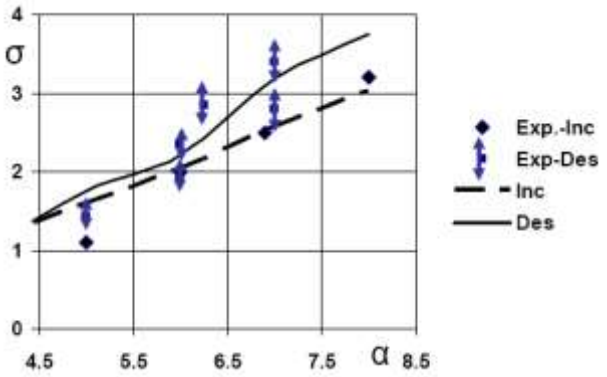


**Figure 18** Computed [16] and measured [7] cavitation inception and desinence numbers for the steady water tunnel flows around Cav2003

Computed $\sigma_d$ for Cav2003 is compared in Fig.19 in with the measurements [6]. There is no coincidence in this figure. On the other hand, the data [6] are not very close to the data [7] presented in Fig.18 for the hydrofoil Cav2003 tested in another facility.

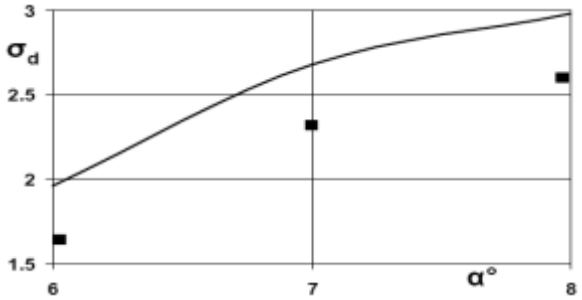


**Figure 19** Comparison of computed (line) and measured [6] cavitation desinence number for the steel hydrofoil.

The capability of the presented computed results to follow the experimental trends is shown in general, but because of the insufficiency of information on the incoming flow, there is no possibility to directly apply such computations to prediction of the material effect on cavitation inception and desinence. Instead the material influence can be estimated qualitatively by comparison of some composed ratios. Let us introduce *dσ* as the difference between cavitation inception (or desinence) numbers for the aluminum hydrofoil and the steel hydrofoil. Then the ratios plotted in Fig.20 can be used as the qualitative comparative criterion for the presented numerical analysis and experimental data. One can see a very good result for cavitation desinence and a barely satisfactory trend for cavitation inception.

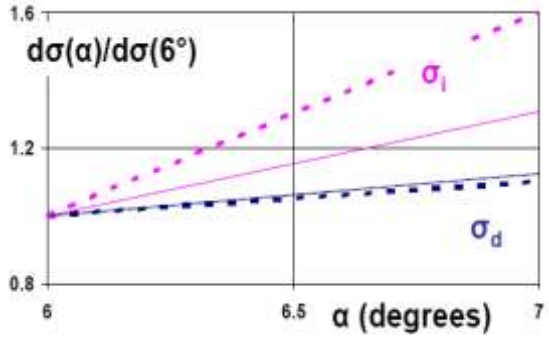


**Figure 20** Hydrofoil material impact on $\sigma_d$ and $\sigma_i$; dashed lines show data [6], solid – numerical results

A generalization of the provided estimations for larger hydrofoils or blades would first require corrections to the incoming flow spectrum. In particular, for the full-scale conditions, the inflow perturbation must be coordinate-dependent.

## CONCLUSIONS

The provided numerical analysis manifests that the hydrofoil/blade material can substantially impact its cavitation inception and desinence just due to the hydroelastic effects. Unlike to the study [9], no torsion-caused flow perturbations were found here, but deflection of the hydrofoil trailing edge due to fluid-structure interaction plays the major role.

This hydrofoil (or blade) material impact should be considered among other factors listed as influencing cavitation inception (as were listed, for example, in [22]). The parameters predetermining this impact (hydrofoil density, elasticity modulus, and turbulence intensity) should be noted in the descriptions of the future experimental studies.

Further, the provided results prompt that taking into account complex influences of various factors in model tests and in full-scale flows one may try to fit model test results simply by controlling the thickness of the model trailing edge.

## REFERENCES

[1] Knapp, R.T., Daily, J.W. and Hammitt, F.G., 1970, *Cavitation*, McGraw-Hill

[2] Hsiao, C-T., Ma, J. and Chahine, G.L., 2014, "Multi-Scale Two-Phase Flow Modeling of Sheet and Cloud Cavitation", 30th Symp. Naval Hydrodynamics, Hobart, Australia

[3] Arakeri, V.H., 1975, "Viscous effects on the position of cavitation separation from smooth bodies", J. Fluid Mech., **68**, 779-799

[4] Ivanov, A.N., Amromin, E.L., 1980, "Ideal cavitation and real cavitating flows". Chapter 6 in: *Hydrodynamics of Developed Cavitating Flows* by Ivanov, A.N, Sudostroenie, Leningrad (in Russian)

[5] Leder, A.T. and Ceccio, S.L., 1998, "Examination of the flow near the leading edge of attached cavitation. Part 1: Detachment of two-dimensional and axisymmetric cavities", J. Fluid Mech., **376**, 61-90

[6] Williams, M., Kawakami, E., Amromin, E. and Arndt, R., 2009, "Effect of surface characteristics on hydrofoil cavitation", 7th Int. Symp. Cavitation, Ann Arbor

[7] Courtier-Delgosha, O., Deniset, F., Astolfi, J.A. and Leroux, J-B., 2007, "Numerical Prediction of Cavitating Flow on a Two-Dimensional Symmetrical Hydrofoil and Comparison to Experiments", ASME J. Fluids Eng.**129**, 279-292

[8] Amromin, E.L., 2007, "Determination of cavity detachment for sheet cavitation". ASME J. Fluids Eng., **129**, 1105-1111

[9] Ausoni, P., Farhat,M., Escaler, X., Egusquiza, E. and Avellan, F., 2007, "Cavitation Influence on von Kármán Vortex Shedding and Induced Hydrofoil Vibrations", ASME J. Fluids Eng. **129**, 966-973

[10] Akcabay, D.T., Chae, E.J., Young, Y.L., Ducoin, A., Astolfi, J.A., 2014, "Cavity induced vibration of flexible hydrofoils", J. Fluids Structures, **49**, 463-484

[11] Birnbaum, W., 1924, "Das ebene Problem des schlagenden Flugels", Zeitschrift Ang. Math. Mech., **4**, 277-292 (in German)

[12] Amromin, E.L. and Kovinskaya, S.I., 2000, "Vibration of cavitating elastic wing in a periodically perturbed flow: excitation of sub-harmonics", J. Fluids Structures, **14**, 735-747

[13] Blake, W.K., 1986, *Mechanics of Flow-Induced Sound and Vibration*, Academic Press

[14] Ducoin, A., Astolfi, J.A., Sigrist, J-F., 2012, "An experimental analysis of fluid structure interaction on a flexible hydrofoil in various flow regimes including cavitating flow", European Journal of Mechanics B/Fluids, **38**, 63-74

[15] De La Torre, O., Escaler, X., Egusquiza, E., Farhat, M., 2013, "Experimental investigation of added mass effects on a hydrofoil under cavitation conditions", J. Fluids Structures, **39**, 173-187

[16] Amromin, E.L., 2014. "Development and validation of CFD models for initial stages of cavitation", ASME J. Fluids Eng. **136**, 081303-1:8

[17] Mishkevich, V.G., 1995, "Scale and roughness effects in ship performances in designer's viewpoint", Marine Technology, **32,** 126-131

[18] Arndt, R.E.A., 1981, "Cavitation in fluid machinery and hydraulic structures", Ann. Rev. Fluid Mech. **13,** 273-328

[19] Amromin, E.L. 2013, "Analysis of airfoil stall with a modification of viscous-inviscid interaction concept "ASME J. Fluids Eng., **135,** 051105-1:7

[20] Malley, K.O., Fitt, A.D., Jones, T.V., Ockendon, J.K. and Wilmott, P., 1991, "Model for high-Reynolds number flow down a step". J. Fluid Mech, **222**, 139-155

[21] Simpson, R.L., Agarwal, N.K., Nagaushana, K.A. & Olcmen, S., 1990, "Spectral Measurements and Other Features of Separating Turbulent Flows", AIAA Journ. **28**, 446-452

[22] Gindroz, B., Billet, M. L., 1998, "Influence of the Nuclei on the Cavitation Inception for Different Types of Cavitation on Ship Propellers", ASME J. Fluids Eng. **120**, 171-178